Appl. Phys. B 78, 983–988 (2004)
DOI: 10.1007/s00340-004-1430-9

Applied Physics B
Lasers and Optics

Invited paper

Recent developments in X-UV optics and X-UV diagnostics

PH. ZEITOUN[1,✉]
PH. BALCOU[2]
S. BUCOURT[3]
F. DELMOTTE[4]
G. DOVILLAIRE[3]
D. DOUILLET[2]
J. DUNN[5]
G. FAIVRE[1]
M. FAJARDO[1]
K.A. GOLDBERG[6]
S. HUBERT[2,1]
J.R. HUNTER[5]
M. IDIR[1]
S. JACQUEMOT[7]
S. KAZAMIAS[2]
S. LE PAPE[1]
X. LEVECQ[3]
C.L.S. LEWIS[8]
R. MARMORET[7]
P. MERCÈRE[1]
A.S. MORLENS[1]
P.P. NAULLEAU[6]
M.F. RAVET[4]
C. RÉMOND[7]
J.J. ROCCA[9]
R.F. SMITH[5]
P. TROUSSEL[7]
C. VALENTIN[2]
L. VANBOSTAL[1]

[1] Laboratoire d'Interaction du rayonnement X avec la Matière, Université Paris-Sud, Bât 350, 91405 Orsay, France
[2] Laboratoire d'Optique Appliquée, ENSTA, Chemin de La Hunière, 91761 Palaiseau, France
[3] Imagine Optic, 18 rue Charles de Gaulle, 91400 Orsay, France
[4] Laboratoire Charles Fabbry de l'Institut d'Optique, CNRS-UMR 8501, Bât 503, Centre Scientifique, 91403 Orsay, France
[5] Lawrence Livermore National Laboratory, Livermore, CA 94551, USA
[6] Center for X-ray Optics, Lawrence Berkeley National Laboratory, 1 Cyclotron Road, Berkeley, CA 94720, USA
[7] Commissariat á l'Énergie Atomique, BP 2, 91680 Bruyères-le-Chatel, France
[8] School of Mathematics and Physics, The Queen's University of Belfast, Belfast BT7 1NN, UK
[9] NSF ERC for Extreme Ultraviolet Science and Technology and Department of Electrical and Computer Engineering, Colorado State University, Fort Collins, CO 80523-1373, USA

Received: 31 October 2003
Published online: 19 March 2004 •

ABSTRACT Metrology of XUV beams (X-ray lasers, high-harmonic generation and VUV free-electron lasers) is of crucial importance for the development of applications. We have thus developed several new optical systems enabling us to measure the optical properties of XUV beams. By use of a Michelson interferometer working as a Fourier-transform spectrometer, the line shapes of different X-ray lasers have been measured with a very high accuracy ($\Delta\lambda/\lambda \sim 10^{-6}$). Achievement of the first XUV wavefront sensor has enabled us to measure the beam quality of laser-pumped as well as discharge-pumped X-ray lasers. A capillary discharge X-ray laser has demonstrated a very good wavefront allowing us to achieve an intensity as high as 3×10^{14} W cm^{-2} by focusing with a $f = 5$ cm mirror. The sensor accuracy has been measured using a calibrated spherical wave generated by diffraction. The accuracy has been estimated to be as good as $\lambda/120$ at 13 nm. Commercial developments are underway. At Laboratoire d'Optique Appliquée, we are setting up a new beamline based on high-harmonic generation in order to start the femtosecond, coherent XUV optic.

PACS 07.85.Nc;32.70.Jz;41.50.+h;42.15.Dp;42.55.Vc;52.70.La

1 Introduction

For several years, the laser-driven XUV source community has faced a new challenge: make these sources as easy of use for applications as conventional XUV sources (i.e. synchrotrons). The success of applications, not all of them, often relies on the XUV optics used for beam metrology or shaping or for the application itself. Recently, progress has covered several fields of XUV optics[1] from interferential multilayer coatings to interferometers or wavefront sensors. Two applications have led the developments: EUV lithography [1] and spatial telescopes [2]. Solar telescopes aim to achieve monochromatic images of the Sun, with wavelengths that correspond mainly to emission lines of Fe and He, which are in the 15–40-nm range. Note that the interferential multilayer coatings developed for solar telescopes are in the wavelength range of interest for high-harmonic or X-ray laser communities. Furthermore, the mirrors of these telescopes have to be very spectrally selective for discriminating the emission of spectrally close lines. Measurements on the LURE synchrotron showed a good spectral selectivity for mirrors around 10–30 nm [2]. Work has also been conducted on using new materials (B_4C/Si, Sc/Si, etc.) in order to achieve higher reflectivity at longer wavelength (≥ 30 nm) than the classical

✉ Fax: +33-1/6931-9898, E-mail: phillippe.zeitoun@ensta.fr

[1] XUV light ranges typically from 4 to 60 nm.

Mo/Si multilayer. Tests have been done at Saclay using the HHG facility and on the LURE synchrotron, showing a good extinction ratio between adjacent harmonics.

Another dynamic area of research is the phase (spatial or temporal) metrology and control of optics or XUV beams. This is related to the development of interferometers used in a wide range of applications and also to the aim of tightly focusing the XUV beams for achieving very large intensities. This paper will describe the most recent works achieved on phase metrology in the XUV, at the Laboratoire d'Interaction du rayonnement X avec la Matière (LIXAM) through several collaborations.

2 XUV Fourier-transform spectroscopy using a Michelson interferometer

From the first experiments of Da Silva and collaborators [3] or Joyeux et al. [4], many interferometers have been set up (Mach–Zehnder [3], Fresnel bimirror [4], Lloyds [5], SMARTT [6], etc.). At LIXAM/LCFIO, we have chosen to develop the so-called Michelson interferometer [7] (Fig. 1). The geometry allows us to easily and under vacuum change the fringe parameters, i.e. spacing and orientation. This is an important improvement compared to previous interferometers. Indeed, while probing a plasma the strong variation of the density gradients may locally cause a fringe mixing, preventing us from retrieving the phase and then the density. The solution consists in increasing the fringe spacing, which is most often done by fully re-aligning the interferometer taking several hours or days. With the Michelson interferometer fringes may be optimized under vacuum by simply tilting a mirror with a motorized stage. The second reason for preferring the Michelson interferometer comes from its common use, in the visible-wavelength range, as a highly resolving spectrometer using the Fourier-transform-spectroscopy (FTS) technique. This part of the paper will show the first results achieved with our Michelson interferometer on the FTS.

This first study was performed with the 13.89-nm, collisionally excited, Ni-like silver X-ray laser (XRL) running at the Laboratoire pour l'Utilisation des Lasers Intenses (LULI) in France. The XRL was produced by irradiating a massive, 2-cm-wide, silver target with six IR beams ($\lambda = 1.054\,\mu$m, $\Delta t_{\mathrm{FWHM}} = 130$ ps) at an intensity on target of $3 \times 10^{13}\,\mathrm{W\,cm^{-2}}$. The highly ionized laser-produced plasma undergoes a population inversion by electronic collisional excitation. Spontaneously emitted rays are then amplified in single pass by traveling along the whole plasma column. The XRL has an output energy ranging from 50 to 400 μJ [8], a measured divergence near $1.9 \times 5\,\mathrm{mrad}^2$ and a refraction angle of 4 mrad in the horizontal plane. Displayed in Fig. 2 is an interferogram obtained for equilibrated arms, i.e. the path-length difference is close to 0 μm. We may observe that the fringes are straight over the major part of the view field but are distorted at the edges. As one can see in Fig. 1, the Michelson interferometer is composed of two flat mirrors, with relatively good flatness, and a beam splitter. This element is the most critical since it is composed of a thin Si_3N_4 membrane, 80-nm thick, $5 \times 5\,\mathrm{mm}^2$, coated on both sides by four or five Mo/Si bilayers. Since these beam splitters have a low internal stress, their flatness is deteriorated at the edges, leading to the observed fringe deformation.

Thanks to the acquisition of a new, fast magnetron sputtering coating machine by the PRaXO [9] consortium, an extensive study has been done aiming to increase the beamsplitter flatness. The key point for achieving a flat beam splitter is the membrane internal stress that has to be kept as high as possible. The membranes have a typical internal stress of 1 GPa, dropping to about 100 MPa after being coated with Mo/Si using the 'old' ion beam sputtering machine. Several coating parameters have been studied for their influence on the stress by using the magnetron sputtering technique: number of periods, ratio between Mo and Si, power of the generators, etc. It seems that the most important parameter is the ratio between Mo and Si thicknesses, despite the fact that we can not vary it over a wide range because it has a strong in-

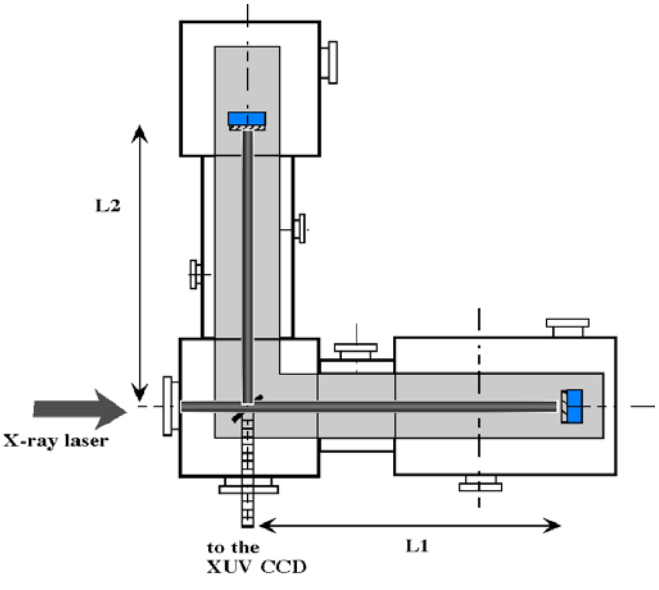

FIGURE 1 Schematic drawing of the Michelson interferometer setup for the LULI experiment. L1 and L2 are the path lengths for each arm

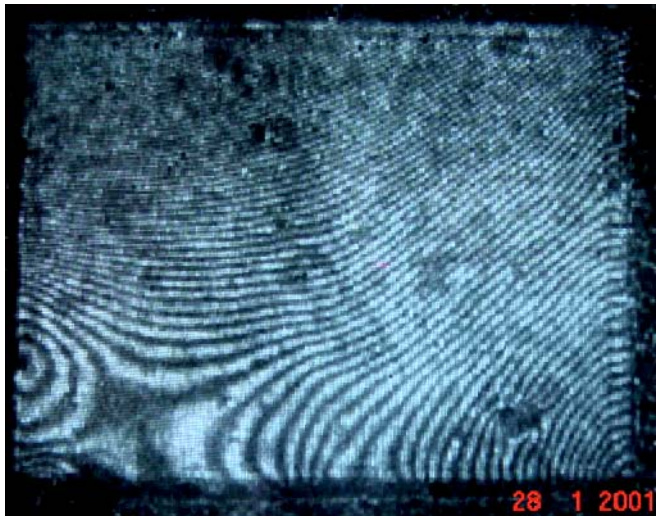

FIGURE 2 Interferogram achieved with the Ni-like Ag X-ray laser. The interferometer arms were equilibrated, leading to highly contrasted fringes (up to 90%)

fluence on the peak reflectivity. After tests, we succeeded in keeping the beam-splitter stress to about 850 MPa. The flatness was then measured with a commercial visible wavefront sensor having an accuracy of about 4 nm. This technique is not as accurate as using an XUV beam for generating interference fringes, but has the interest of being very versatile. The flatness measured over the full aperture has been strongly improved from 78 ± 8 nm root-mean square (rms) with the old coating to 25 ± 5 nm rms now. It should be noted that the useful size (where the beam splitter will not distort the XUV interference fringes, i.e. a flatness around 4 nm) has been increased from about 1 mm^2 to 3 mm^2.

The method for deducing spectral lines by recording the intensity of interference fringes was pioneered by A.A. Michelson in 1891 [10]. By smoothly translating one end mirror of this interferometer (Fig. 1) the optical path difference δ between the beams reflecting off the two mirrors vary continuously, producing an interferogram. The measured fringe visibility, V, is equal to the magnitude of the complex degree of temporal coherence, $\gamma(\tau)$, of the illumination beam. This quantity is directly related to the power spectral density $J(\nu)$ of the beam through a Fourier-transform relation (Wiener–Khinchin theorem [11]):

$$J(\nu) = \int_0^\infty \gamma(\tau)\, \mathrm{e}^{\mathrm{i}2\pi\nu\tau} \mathrm{d}\tau, \tag{1}$$

where $\tau\ (= \delta/c)$ is the relative time delay. Consequently, obtaining the Fourier transform of the variation of fringe visibility versus optical path difference allows us to deduce the spectral line shape of a given source. We may remark that the ease of changing the Michelson interferometer setup is crucial here for scanning the contrast curve.

The Michelson interferometer was initially used at LULI, France in combination with an X-ray laser pumped by a 130-ps, IR laser. The second run of experiments has been performed in collaboration with J. Dunn's group from Lawrence Livermore National Laboratory (LLNL), USA. The Ni-like Pd 14.68-nm X-ray laser beam was generated using two laser beams at 1054-nm wavelength from the compact multipulse terawatt (COMET) laser facility at LLNL [12]. A saturated X-ray laser was achieved with a combination of a 600-ps-long pulse (2 J, 2×10^{11} W cm^{-2}) and a 13-ps (5 J, 3×10^{13} W cm^{-2}) main heating pulse. The short pulse arrived 700 ps peak-to-peak after the long pulse. For some shots the duration of the picosecond pulse was shortened to 6 ps (5 J, 6×10^{13} W cm^{-2}). In Fig. 3, there is displayed the measured fringe visibility curves for X-ray lasers pumped by a 6- or a 13-ps driving laser. It is interesting to note that the curve width is somehow larger for the longer driving pulse, leading to a smaller line width, as coming from different plasma conditions during XRL emission and amplification.

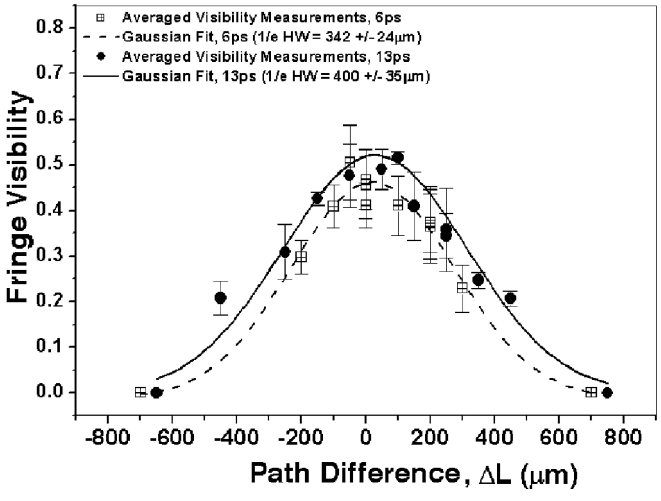

FIGURE 3 Variation of fringe visibility with path difference between the two arms of the interferometer for 6-ps (*open symbols*) and 13-ps (*closed symbols*) heating pulses. Each *data point* is the average visibility for a given shot taken from nine separate measurements across the interferogram. *Error bars* represent one standard deviation. The data points are fitted by a Gaussian curve with a 1/e half-width (HW) of 400 μm ± 35 μm (*solid line*, 13 ps) and 342 μm ± 24 μm (*dashed line*, 6 ps)

3 XUV wavefront measurements

During recent years, wavefront measurement has been one of the major fields of research for visible lasers. Indeed, in the race to achieve higher and higher intensity, no one may accept a focal spot having most of the energy spread out of the central spot. For the visible-wavelength range, most of the recent developments in improving the wavefront of a focused beam have been concentrated on the laser itself, because it is quite easy to buy a diffraction-limited optic. We would like to recall that, according to the Marechal criterion, a diffraction-limited beam should have a wavefront error lower than $\lambda/14$ rms, λ being the laser wavelength. However, due to the strong wavelength shortening it is quite difficult to make a diffraction-limited XUV optic. Researches on EUV lithography [1] have boasted the development of high-quality optics but they are still very expensive and take a long time to make.

Several types of wavefront sensors have been developed so far in the visible range. Interferometers intrinsically measure a wavefront. However, most of them recombine the beam onto itself, making difficult the achievement of an absolute phase map. Also, the fringe spacing is generally linked to the wavelength, thus requiring realignment of the interferometer after any wavelength change. This makes interferometers poorly versatile. Another kind of wavefront sensor is based on ray propagation. The principle is displayed in Fig. 4. The beam is sampled by splitting it into many beamlets (by using a hole or a lens array). All the beamlets are considered to have a flat but tilted wavefront. The position of each beamlet spot on the detector gives directly the angle of the wavefront tilt at the position of the hole or lens array. Then, if the beam is coherent, we may integrate all the wave vectors and reconstruct the wavefront. If the beam is partially coherent this last step has no physical meaning and then we just achieve a map of the wave vectors. Hartmann (hole array) and Shack–Hartmann (lens array) wavefront sensors are very simple and robust. For Hartmann sensors, there is no chromatic effect, which makes them very versatile.

Some years ago we developed the first XUV wavefront sensor based on the Shack–Hartmann technique [13]. Fresnel lenses (also called zone plates) have been used, which

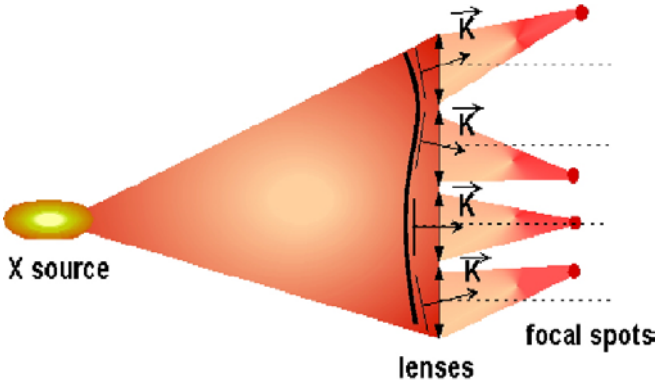

FIGURE 4 Schematic diagram of a Shack–Hartmann wavefront sensor. The local wavefronts as well as the local wave vectors are displayed

are diffractive, focusing optics. Due to the high absorption of most materials in the wavelength range of interest we use reflective Fresnel lenses. These lenses are made by etching a photo-resist coated onto a silicate substrate, the ellipsoids being written by an electron beam. After the etching phase, the whole substrate is coated with a reflective interferential multilayer (Mo/Si). The detector was a back-illuminated, thinned CCD sensitive to XUV light.

Our first study consisted in measuring the wavefront of several collisional X-ray lasers. We have worked with both laser-pumped and capillary discharge XRLs. For laser-pumped XRLs we measured the beam quality of the XRLs pumped by 600-ps, 130-ps and 20-fs infrared lasers [14]. In this paper we will discuss only the Ne-like Ar capillary discharge XRL emitting at 46.9 nm developed at Colorado State University [15].

We first study the influence of the plasma length on the wavefront quality. In Fig. 5 there is displayed the wavefront (a) and the intensity maps (b) as measured by the wavefront sensor for a 18-cm-long plasma. For this capillary length the XRL just reaches the saturation regime, which for the excitation conditions used in this experiment is reached for plasma column lengths of 14–15 cm. We observed a smooth but strongly distorted phase. The intensity is annular.

From these two items of data we may fully reconstruct the XRL electric field and then by Fourier transformation estimate the intensity distribution at a theoretical focal plane. We consider here a 5-cm focal length. The intensity map at the focal plane is displayed in Fig. 6. We may observe a central peak surrounded by several smaller peaks and also light spread far

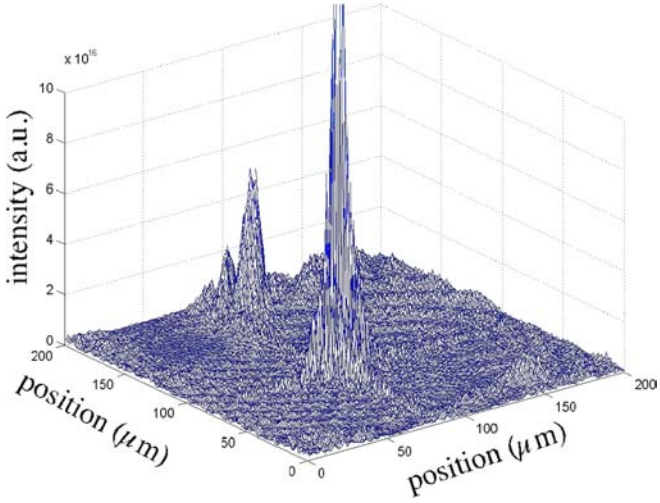

FIGURE 6 Theoretical intensity distribution at the focal plane of a perfect focusing optic with $f = 5$ cm and considering the beam parameters displayed in Fig. 5

away. We then estimated that about 5% of the incident energy was in the central peak of 3 μm in diameter, agreeing quite well with the measurement achieved by Benware and collaborators in the same conditions [16].

An increase of the plasma column length to 36 cm significantly improves the beam, as observed in the map displayed in Fig. 7a, which shows a smooth wavefront having a distortion lower than 1.5λ. It is interesting to note that the wavefront is roughly spherical and divergent. The Fourier transform of the associated electric field (wavefront Fig. 7a and intensity Fig. 7b) shows a clean focal spot, 0.5 μm FWHM (Fig. 7c). The intensity is then estimated to be around 513 W cm^{-2}.

One of the main difficulties while using a Hartmann or Shack–Hartmann wavefront sensor is the need of precalibrating it. Commonly to calibrate the sensor one uses a reference wave, often generated by the diffraction of an XUV beam onto a pinhole. The typical size of the pinhole is around 1 μm depending on the diffracted-beam optical aperture needed. Previous work has shown that the wavefront is better than $\lambda/100$ over a disk, half the diameter of the Airy ring [6], centered on it. Attention has to be paid to that phase since the accuracy of the wavefront sensor will be obviously limited by the quality of the calibration wave. It is preferable to focus the incoming light onto the pinhole to increase the transmitted power. Consequently, a high-power XUV source

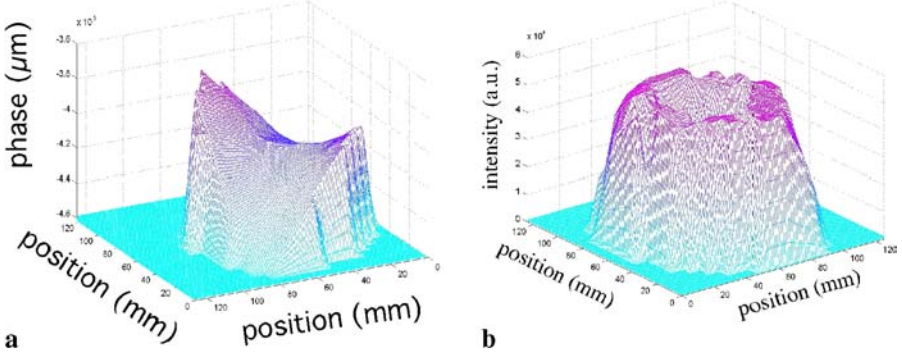

FIGURE 5 XRL wavefront (**a**) and intensity (**b**) maps as measured at 2.5 m from the end of a 18-cm capillary discharge X-ray laser

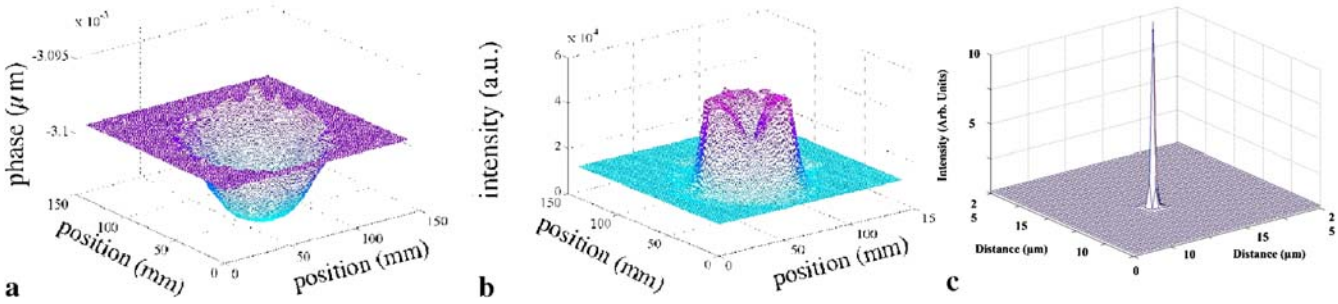

FIGURE 7 Wavefront (**a**) and intensity (**b**) maps of a 36-cm-long capillary X-ray laser. **c** shows the theoretical focal spot as calculated with these experimental data and considering a $f = 5$ cm focusing mirror

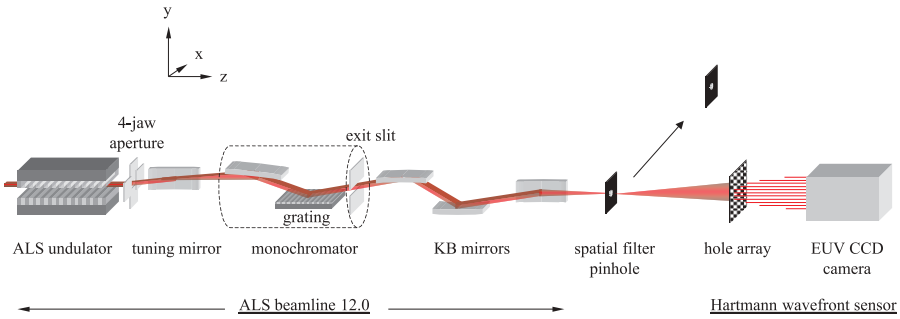

FIGURE 8 Diagram of the beamline 12.0 at the ALS synchrotron facility as it was used for Hartmann-sensor calibration. The pinhole was inserted for calibration and was removed for measurement of the beamline wavefront

having a relatively good wavefront is required for calibrating a wavefront sensor. For this task, under a collaboration between Imagine Optic, Center for X-ray Optics and LIXAM, we used the beamline 12.0 of the third-generation synchrotron ALS. This beamline is based on an undulator emitting a high-power beam from 6 to 25 nm. Beamline 12.0 being commonly used for interferometric measurement with a point-source interferometer, most of the setup was already existing (pre-focusing, pinhole, etc.). The diagram displayed in Fig. 8 shows the beamline geometry as well as the implementation of the wavefront sensor. The beam is first monochromatized and then focused onto the pinhole by a Kirkpatrick–Baez optic. For this work, we used a hole array to sample the beam. The undulator was mainly run at 13 nm but we also tested the wavefront sensor from 6 to 25 nm.

Estimation of the sensor accuracy has been made by comparing the wavefronts generated by the diffraction of the pinhole on two independent measurements. The measured accuracy is around $\lambda/120$ rms at 13 nm with a sensitivity exceeding $\lambda/1500$ rms. Note that to our knowledge the best XUV interferometers demonstrated an accuracy of around $\lambda/300$. Over the 6–25-nm wavelength range, no noticeable loss of accuracy has been observed.

After the calibration phase, the pinhole was removed, enabling us to measure the wavefront of the unfiltered beamline. The result is displayed in Fig. 9a. We observed that the main aberration is the astigmatism probably coming from a slight misalignment of one or two mirrors of the Kirpatrick–Baez optic. From the wavefront measurement, Imagine Optic's software calculates the focal spot (Fig. 9b), which is in good agreement with direct measurements.

Further development of XUV wavefront sensors, particularly their commercialization, will require us to easily access a source like the beamline 12.0 having a 'perfect' wavefront for calibration. Beamline 12.0 being heavily used for lithography projects, the access time will be low. We are thus setting up a coherent XUV beamline at the Laboratoire d'Optique Appliquée, France. As pointed out the main parameters are the wavefront quality, the average power and the possibility to tune the wavelength, typically from 10 to 60 nm. At the

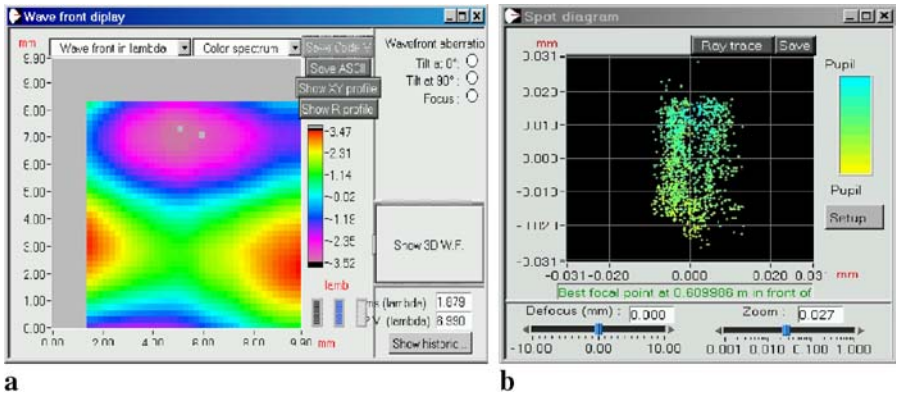

FIGURE 9 Image of the experimental beamline 12.0 wavefront (**a**) and the focal spot (**b**) as calculated from the experimental data

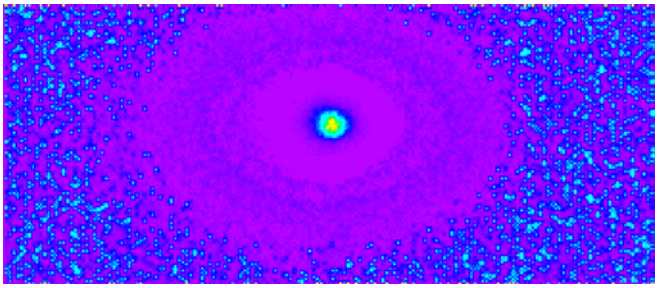

FIGURE 10 Corrected image of the focal spot obtained by focusing the HHG with an off-axis parabola ($f = 7$ cm) onto a YAG : Ce luminescent crystal. The focal spot diameter is around 2.5 μm

moment X-ray lasers do not correspond to our needs (low repetition rate, low average power, no tunability). High-harmonic generation (HHG) corresponds quite well to all our requirements. Typically on beamline 12.0 the power is around 10 μW at 13 nm after the spatial filter and, from previous LOA (Laboratoire d'Optique Appliquée.) work [17], it is estimated at 6 μW with the HHG at 30 nm. The power drops to 6 nW around 13 nm. We may expect to increase this value by more than one order of magnitude after optimization and/or by increasing the laser repetition rate. Enhancement of the output power is linked to the quality of the spot while focusing the HHG onto the pinhole.

Tight focusing of the HHG requires the use of a good-quality optic for keeping the wavefront as good as possible. For generating a focal spot with a diameter around 1 μm, the focal length has to be short (5–10 cm). Also, due to the need to place a pinhole at the focal spot, the beam cannot go downstream. Short focal length, grazing-incidence mirrors are generally not so good, leading to a distorted focal spot [18]. Sophisticated grazing-incidence focusing optics correcting the aberrations are feasible but are quite expensive. One of them will be set up for the future LOA/LIXAM beamline. However, for the first work we decided to use an off-axis parabola enabling us to shift, without distortion, the focal spot out from the incoming beam path. For the sake of ease of alignment the full parabola was polished, while just a small part (off-axis) has been polished to the required quality ($\lambda/30$ rms, $\lambda = 632.8$ nm). By placing a luminescent crystal (YAG : Ce) in place of the focal spot we measured the intensity repartition. The parabola was coated with a 1000-Å Cr layer in order to keep the focused intensity at a low level, preventing damage to the crystal. The YAG green emission was magnified by a lens doublet ($\times 30$) and recorded on a visible CCD. Due to the YAG non-linear response versus HHG intensity the raw image has been corrected (Fig. 10). The spot is circular, showing that aberrations have been kept at a negligible level. The spot diameter is around 2.5 μm.

4 Conclusion

Phase metrology is key for applications based on the use of the new XUV sources. We have developed XUV beam splitters through the realization of a Michelson interferometer. Currently, the beam-splitter flatness is better than 4 nm over a 3×3 mm^2 surface. The Michelson interferometer has been used to conduct a large study of X-ray laser line shape (Fourier-transform spectroscopy), considering several conditions of pumping (long pulse and transient). XUV FTS is opening a wide range of applications.

We also developed the first XUV wavefront sensor enabling us to study the beam quality of many X-ray lasers. Capillary discharge XRLs have a very good wavefront, ensuring that tight focusing is possible. Most recent developments of XUV wavefront sensors have consisted in measuring their absolute accuracy ($\lambda/120$ at 13 nm). The first step for setting up a coherent XUV optic beamline has been to demonstrate that micrometer focusing is possible with HHG.

REFERENCES

1 For more detail, please refer to M. Schmidt et al. [these proceedings]
2 M.F. Ravet et al.: Proc. SPIE **5250**, 12 (2003)
3 L.B. Da Silva et al.: Phys. Rev. Lett. **74**, 3991 (1995)
4 D. Joyeux, F. Polack, D. Phalippou: Rev. Sci. Instrum. **70**, 2921 (1999)
5 J.J. Rocca et al.: Opt. Lett. **24**, 420 (1999); B. Rus et al.: in *Proc. 8th Int. Conf. X-ray Lasers, Aspen, 2002*, ed. by J.J. Rocca, J. Dunn, S. Suckewer (AIP Conf. Proc. **641**) (American Institute of Physics) p. 522
6 H. Medecki et al.: Opt. Lett. **21**, 1526 (1996)
7 F. Delmotte et al.: Appl. Opt. **41**, 5905 (2002)
8 S. Sebban et al.: Phys. Rev. A **61**, 043 810-1 (2000)
9 Pôle Rayons X d'Orsay is composed of several laboratories working on XUV optics
10 M.E. Kelin, T.E. Furtak: *Optics*, 2nd edn. (John Wiley and Sons ed. 1986)
11 J.W. Goodman: *Statistical Optics* (Wiley, New York 1985) p. 74
12 J. Dunn et al.: Phys. Rev. Lett. **80**, 2825 (1998)
13 S. le Pape et al.: Phys. Rev. Lett. **88**, 18 (2002)
14 S. le Pape et al.: Proc. SPIE **4505**, 221 (2001)
15 C. Macchietto et al.: Opt. Lett. **24**, 1115 (1999)
16 B.R. Benware et al.: Opt. Lett. **24**, 1714 (1999)
17 S. Kazamias et al.: Eur. Phys. J. D **21**, 353 (2002)
18 C. Valentin et al.: Opt. Lett **28**, 12 (2003)